AIAA 80-0969R

Transmission of High-Frequency Sound Waves Through a Slug Flow Jet

S. P. Parthasarathy* and A. Vijayaraghavan†
Jet Propulsion Laboratory, California Institute of Technology, Pasadena, Calif.

An analysis has been performed of sound waves which propagate in a pipe with gas flow. At the pipe exit these waves are partially reflected and the remainder are diffracted. The analysis is carried out by resolving the sound at the exit into its Fourier components and then continuing the solution, which is a combination of elementary plane waves, beyond the exit. These waves are of two types: homogeneous waves that propagate to infinity, and inhomogeneous waves with complex wave numbers that decay. The reflected waves are evaluated from the inhomogeneous waves. At the boundary of the jet, refraction of the elementary plane waves is accounted for and the far-field sound is evaluated asymtotically. Comparisons of the theoretical calculations are made with experimental results and with calculations of other theories.

Nomenclature

A	= constant in Eq. (9) defined in terms of B
b	= pipe radius
B	= constant in Eq. (5), a measure of pressure at the pipe exit
c	= speed of sound
f	= function, see Eq. (23)
I	= interference factor
J	= Bessel function of the first kind
k	= wavenumber
M	= Mach number
m	= circumferential mode number
n	= radial mode number
p	= sound pressure
r	= cylindrical radius
R	= polar radius
$\Re$	= pressure reflection coefficient
T	= pressure transmission coefficient
t	= time
U	= flow speed
w	= variable of integration, see Eq. (19)
x,y,z	= Cartesian coordinates
α	= angle in the plane of cross section, see Eq. (6)
δ	= spherical polar angle of the wave vector
θ	= spherical polar angle of position coordinate r
ρ	= density
ϕ	= cylindrical polar coordinate
ϕ_I	= phase in Eq. (29)
ψ	= velocity potential
χ,χ_I	= Hankel transform of pressure, Eqs. (10) and (A2)
ω	= angular frequency

Subscripts and Superscripts

A,B,C	= various regions shown in Fig. 1
m,n	= mode numbers
p	= plenum
x,y,r	= components of vector
$\tilde{\ }$	= near field
$\langle\ \rangle$	= average over cross section

Presented as Paper 80-0969 at the AIAA 16th Aeroacoustics Conference, Hartford, Conn., June 4-6, 1980; submitted July 18, 1980; revision received Dec. 22, 1980.

*Member of the Technical Staff. Member AIAA.
†Member of the Technical Staff.

Introduction

SOUND waves that propagate with the mean flow in a circular pipe undergo reflection and diffraction at the pipe exit. An analysis is presented which consists of a high frequency approximation for the refraction of sound at the vortex sheet region that separates the moving slug-flow jet from the surrounding atmosphere. As in other theories,[1-3] the existence of turbulence in the jet is ignored and, correspondingly, scattering of sound by turbulence is not considered. This analysis may be applied to more complex geometries such as to flows from nozzles and propagation through spreading jets.

Different solutions have been obtained by Munt[1] and Savkar[2] for the problem of sound transmission through a pipe with flow by the use of the Wiener-Hopf technique. Munt's solution contains instability waves and Savkar's does not. Mani[3] solved the same problem for the two-dimensional case by the same technique. These solutions are restricted to the simple geometry for which the Wiener-Hopf technique is suited. They are also quite complicated.

A statistical theory for sound radiation and reflection from a duct without mean flow is given by Cho.[4] In his analysis sound is interpreted as a collection of quasiparticles, i.e., phonons. This method is simple and provides a straightforward interpretation of the physical phenomenon. It can be applied to cases where the Wiener-Hopf technique fails. The calculated results of Cho's theory compare quite favorably with the results of Levine and Schwinger,[5] whose results were also obtained by the Wiener-Hopf technique for a duct with no mean flow.

The present method basically resembles that of Cho but the intuitive phonon concept is not used. It is replaced by the well-known concept[6] of homogeneous and inhomogeneous waves which has a well-defined mathematical representation. It is applicable when flows exist as in this problem where the phonon interpretation is unclear. The sound field at the pipe exit is resolved into a collection of elementary waves of both types. The homogeneous waves with real wavenumbers propagate to infinity and the far-field sound is obtained by superposing all such waves. The inhomogeneous waves with complex wavenumbers decay and do not propagate to infinity. They produce the reflected waves. They correspond, for example, to phonons (concept used by Cho) trapped in the pipe. In Cho's method, the angular distribution of radiation at infinity is considered intuitively to be the Fourier transform of the sound distribution at the pipe exit. This is an analogy of the solution for sound generated by an oscillating piston set in an infinite baffle.[7] By use of the present method it is shown

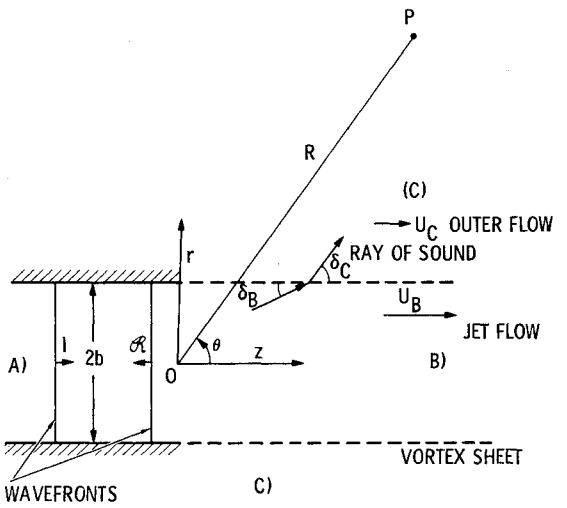

Fig. 1 Sketch that defines the problem of sound transmission through a jet flow exhausting from a circular duct.

that the far field is given by the product of the Fourier transform and other factors including the proper normalizations.

In the present analysis the sound at the pipe exit is resolved into its Fourier components. Each wave propagates out with its own set of propagation constants. The wavenumbers satisfy the appropriate dispersion relations in the various regions. At the interface between the jet and the outer fluid, the laws of refraction are satisfied. The far field is evaluated by superposing these homogeneous elementary waves that propagate to infinity.

Analysis

The problem considered is indicated in Fig. 1. A sound wave propagates downstream in region A in the circular duct and passes through the jet region B to reach region C. Some of the incident sound is also reflected near the exit plane. The sound field at large distances from the exit plane and the reflected wave are to be evaluated for a given incident wave.

Region A

In region A, there exists a uniform axial flow of speed U_A on which sound waves of small amplitude are superposed. The perturbation velocity potential ψ satisfies the convected wave equation

$$\nabla^2\psi+\left(k_A+iM_A\frac{\partial}{\partial z}\right)^2\psi=0 \tag{1}$$

for simple harmonic waves with time dependence expressed by the factor $\exp-i\omega t$. The wavenumber k_A equal to ω/c_A refers to a medium at rest with the properties of region A. The acoustic pressure p is given by

$$p=i\rho_A\omega\left(1+\frac{iM_A}{k_A}\frac{\partial}{\partial z}\right)\psi \tag{2}$$

Consider an incident spinning wave with the pressure p and corresponding ψ given by

$$p=BJ_m(\alpha_{mn}r/b)\exp i(k_{mn}z+m\phi)$$

$$=i\rho_A\omega[1-M_Ak_{mn}/k_A]\psi \tag{3}$$

Note that ψ in Eq. (3) satisfies Eq. (1) if

$$k_{mn}=[-M_Ak_A\pm(k_A^2-b^{-2}(1-M_A^2)\alpha_{mn}^2)^{1/2}]/(1-M_A^2) \tag{4}$$

The positive and negative signs in Eq. (4) correspond to downstream and upstream propagation, respectively. The quantity α_{mn} is the nth zero of the derivative of the Bessel function J_m'. When α_{mn} is larger than $bk_A/(1-M_A^2)^{1/2}$, k_{mn} becomes complex and the mode is cut off. When m and n are both zero, the wave motion is plane.

At the pipe exit $z=0$,

$$p=BJ_m(\alpha_{mn}r/b)\exp im\phi=p(r)\exp im\phi, \text{ for } r<b;$$

$$=0 \text{ for } r>b \tag{5}$$

This field is resolved into its Fourier components. Let

$$x=r\cos\phi \quad y=r\sin\phi \quad k_x=k_r\cos\alpha \quad k_y=k_r\sin\alpha \tag{6}$$

Thus, $p(x,y)=p(r)\exp im\phi$ is the two-dimensional Fourier transform of $\chi(k_x,k_y)=\chi(k_r)\exp im\alpha$. The quantities $p(r)$ and $\chi(k_r)$ are Hankel transforms of each other. It can be shown that[8]

$$\chi(k_r)=i^{-m}\int_0^\infty p(r)J_m(rk_r)r\mathrm{d}r \tag{7}$$

using the expression for $p(r)$ from Eq. (5),

$$\chi(k_r)=i^{-m}\int_0^b BJ_m(\alpha_{mn}r/b)J_m(rk_r)r\mathrm{d}r \tag{8}$$

Following Cho,[4] the Bessel functions can be normalized by choosing

$$B=\sqrt{2}A/b\,|J_m(\alpha_{mn})|\,(1-m^2/\alpha_{mn}^2)^{1/2} \tag{9}$$

and Eq. (8) can be integrated to obtain

$$\chi(k_r)=Ai^{-m}\mathrm{sgn}J_m(\alpha_{mn})\,(1-m^2/\alpha_{mn}^2)^{1/2}$$

$$\times\sqrt{2}b(bk_r)J_m'(bk_r)\,(\alpha_{mn}^2-b^2k_r^2)^{-1} \tag{10}$$

Region B

For $z>0$, the wave motion is described by reintroducing the factor $\exp ik_zz$ which was unity at $z=0$, i.e.,

$$p_B(r)=\frac{1}{2\pi}\iint_{-\infty}^{\infty}\chi(k_r)e^{im\alpha}e^{ik\cdot r}\mathrm{d}k_x\mathrm{d}k_y \tag{11}$$

It is seen that $p_B(r)$ is expressed as a combination of elementary plane waves $\exp ik\cdot r$ of amplitude densities $\chi(k_r)\exp im\alpha$. The wavenumber k_z is not constant in Eq. (11) but varies such that the dispersion relation in Eq. (13) is satisfied in region B.

Equation (11) represents the sound field for the case when there is a uniform flow outside the exit as would occur when $U_C=U_B$ in Fig. 1. The presence of the vortex sheet introduces reflections that have to be considered. However, only the pressure field in region C outside the jet is of particular interest in the problem under consideration and this can be evaluated without calculating the pressure field in region B for large values of z. Equation (11) can be considered to be valid in the immediate vicinity of the pipe exit, i.e., just outside the exit where it represents the primary wave. This wave will undergo multiple reflections and refractions at the vortex sheet that will be evaluated later.

It is more convenient to describe p_B in polar coordinates by choosing

$$r=R\sin\theta \quad z=R\cos\theta \quad k_r=k_B\sin\delta \quad k_z=k_B\cos\delta$$

The quantity

$$k\cdot r=k_xx+k_yy+k_zz=k_BR[\sin\delta\sin\theta\cos(\alpha-\phi)+\cos\delta\cos\theta]$$

The double integral in Eq. (11) is expressed in terms of k_r and α and the integration over α is performed. This yields the single integral for p_B.

$$p_B(r) = \int_0^\infty i^{-m}\chi(k_B\sin\delta)J_m(k_BR\sin\delta\sin\theta)$$

$$\times\exp(ik_BR\cos\delta\cos\theta + im\phi)k_B\sin\delta\mathrm{d}(k_B\sin\delta) \quad (12)$$

In Eq. (12), δ refers to δ_B. The relation between ω and k_B in the jet is

$$\omega = k_Bc_B + U_Bk_B\cos\delta_B \quad (13)$$

Region C

The elementary plane waves expressed by $\exp i(k_BR\cos\delta\cos\theta + m\phi)$ are transmitted across the vortex sheet. At high angles of incidence the transmission coefficient is near unity. At low angles, significant reflections occur. Also, in the present model of smooth parallel jet boundaries, multiple reflections and wave interference occur. The factor by which the pressure amplitude is changed on passage through the vortex sheet is indicated by $I(\delta_B)$. The expression for I is given in a subsequent part of the analysis.

Across the vortex sheet, Snell's law applies.

$$k_B\cos\delta_B = k_C\cos\delta_C \quad (14)$$

Here,

$$\omega = k_Cc_C + U_Ck_C\cos\delta_C \quad (15)$$

The results for the case with no outer flow are of particular interest because most of the experiments have been conducted without the outer flow. Therefore, only the case $U_C = 0$ is considered. Also, for cold jets, $c_B = c_C$. With these assumptions, quantities pertaining to region B are replaced by those referring to region C. From Eqs. (13-15)

$$k_B = k_C(1 - M_B\cos\delta_C) \quad (16)$$

$$k_B\sin\delta_B = k_Cw \quad (17)$$

$$w = \{(1 - M_B\cos\delta_C)^2 - \cos^2\delta_C\}^{1/2} \quad (18)$$

$$\cos\delta_C = \frac{-M_B + \{M_B^2 + (1 - M_B^2)(1 - w^2)\}^{1/2}}{(1 - M_B^2)} \quad (19)$$

Equation (12) now leads to the pressure in region C given by

$$p_C(r) = \int_0^\infty i^{-m}\chi(k_Cw)J_m(k_CwR\sin\theta)\exp im\phi$$

$$\times\exp\{ik_CR\cos\theta[-M_B + \{M_B^2 + (1 - M_B^2)(1 - w^2)\}^{1/2}]$$

$$\div(1 - M_B^2)\}I(w)k_C^2w\mathrm{d}w \quad (20)$$

In Eq. (20) the transmission factor including interference is indicated by $I(w)$. The phase function in the exponent of Eq. (20) remains real when $w \le (1 - M_B^2)^{-1/2}$. Therefore the far-field pressure as $R \to \infty$ is contributed only by values of w from 0 to $w_{\max} = (1 - M_B^2)^{-1/2}$. The rest of the integral produces only a near field which does not propagate to infinity. The part of the integrand that oscillates rapidly as $R \to \infty$ is the product of $J_m(k_CwR\sin\theta)$ and the exponential factor. As $R \to \infty$, J_m may be approximated by

$$J_m(R\sin\theta k_Cw) = \left(\frac{2}{\pi}\right)^{1/2}\frac{\cos(k_CRw\sin\theta - m\pi/2 - \pi/4)}{(k_CwR\sin\theta)^{1/2}} \quad (21)$$

Eq. (21) is substituted into Eq. (20). The cosine in Eq. (21) is the sum of two exponentials. Therefore, $p_C(r)$ is the sum of two integrals $p_{C1}(r)$ and $p_{C2}(r)$.

$$p_{C1}(r) = \int_0^\infty f(w)\exp\frac{irk_C\cos\theta}{(1 - M_B^2)}[-M_B + \{M_B^2 + (1 - M_B^2)$$

$$\times(1 - w^2)\}^{1/2}]\exp i\left[k_CRw\sin\theta - \frac{m\pi}{2} - \frac{\pi}{4}\right]\mathrm{d}w \quad (22)$$

A similar expression exists for $p_{C2}(r)$ in which the second exponential has the opposite phase. In Eq. (22),

$$f(w) = i^{-m}\chi(k_cw)\exp[im\phi]I(w)k_C^2w(2\pi wk_CR\sin\theta)^{-1/2} \quad (23)$$

It can be verified that for a fixed θ, only one of the integrals contributes to $p_C(r)$. The integral in Eq. (22) is evaluated by the method of stationary phase. The stationary point can be shown to be

$$w_s = \sin\theta(1 - M_B^2\sin^2\theta)^{-1/2} \quad (24)$$

Then the far-field pressure can be shown to be

$$p_{C1}(r) = (-1)^{-m+1}\mathrm{sgn}J_m(\alpha_{mn})(1 - m^2\alpha_{mn}^{-2})^{-1/2}$$

$$\times I\left(\frac{\sin\theta}{(1 - M_B^2\sin^2\theta)^{1/2}}\right)\sqrt{2}Ak_Cb^2k_C^2\sin^2\theta(1 - M_B^2\sin^2\theta)^{-1}$$

$$\times\{\alpha_{mn}^2 - b^2k_C^2\sin^2\theta(1 - M_B^2\sin^2\theta)^{-1}\}^{-1}J_m'\left(\frac{bk_C\sin\theta}{(1 - M_B^2\sin^2\theta)^{1/2}}\right)$$

$$\times\{1 + (1 - M_B^2)\tan^2\theta\}^{-1/2}\frac{1}{Rk_C\sin\theta}\exp i\left[\frac{Rk_C}{(1 - M_B^2)}\right.$$

$$\left.\times\{(1 - M_B^2\sin^2\theta)^{1/2} - M_B\cos\theta\} + m\phi - (m+2)\frac{\pi}{2}\right] \quad (25)$$

For negative values of θ, $p_{C2}(r)$ gives the pressure field and the equation is the same as Eq. (25).

Equation (25) simplifies considerably for plane waves where m and n are both zero. Then

$$p_C(r) = \sqrt{2}Ak_CJ_1\left(\frac{bk_C\sin\theta}{(1 - M_B^2\sin^2\theta)^{1/2}}\right)I\left(\frac{\sin\theta}{(1 - M_B^2\sin^2\theta)^{1/2}}\right)$$

$$\times(1 + (1 - M_B^2)\tan^2\theta)^{-1/2}\frac{1}{Rk_C\sin\theta}\exp i\left[\frac{k_CR}{(1 - M_B^2)}\right.$$

$$\left.\times\{(1 - M_B^2\sin^2\theta)^{1/2} - M_B\cos\theta\}\right] \quad (26)$$

This reduces further for the case of no flow where the wave diffraction is described by

$$p_C(r) = \frac{\sqrt{2}Ak_CJ_1(bk_C\sin\theta)}{\sin\theta}\cos\theta\frac{\exp ik_CR}{k_CR} \quad (27)$$

This shows that the far-field spherical wave $(\exp ik_CR)/k_CR$, has an amplitude that is the product of $\cos\theta$ and the Fourier transform of a top hat profile that is $\sqrt{2}Ak_CJ_1(bk_C\sin\theta)/\sin\theta$. The additional $\cos\theta$ factor distinguishes this solution from the solution for a piston set in an infinite baffle. The present solution is a high frequency approximation and gives a zero sound pressure at $\theta = 90$ deg, whether or not $J_1(bk_C)$ is zero. Of course, at high frequencies the difference between the two expressions with and without the $\cos\theta$ factor is small.

The expression for $p_C(r)$ when there is a flow exhibits a nonspherical wavefront as seen by the phase factor in Eq. (26). At $\theta = 0$, the phase is $\exp ik_CR/(1 + M_B)$, showing that the wavefront moves at the increased speed equal to $(1 + M_B)c_C$. At $\theta = \pi/2$, the phase is $\exp ik_CR/(1 - M_B^2)^{1/2}$ which differs slightly from $\exp ik_CR$ by a quantity involving

M_B^2. The explanation for the nonspherical wavefront is that the nonspreading jet continues to carry a portion of the wavefront to $z=\infty$ at $\theta=0$ with supersonic speed $=c_C(1+M_B)$. Real jets decay, $M_B \to 0$ and a spherical wave will be established at large R. The meanflow tends to steepen the frontal radiation pattern. Radiation is present at all angles θ, though perhaps reduced by the interference factor $I(\theta)$. There is no region of silence but only a region of reduced amplitude. This is understandable because the grazing rays in region B emerge at the Mach angle equal to $\cos^{-1}[1/(1+M_B)]$ all along the jet boundary and these reach every position in the far field however small θ may be.

Interference Factor

The factor $I(\theta)$ expressing refraction and multiple beam interference will be discussed next. When plane waves of sound cross the vortex sheet between regions B and C, they are partially transmitted and partially reflected. The pressure transmission coefficient T and pressure reflection coefficient $\mathfrak{R}$ at a plane vortex sheet are given in Chap. 11 of Ref. 9 by

$$\mathfrak{R}+1=T=2(1+\sin^2\delta_C/\sin 2\delta_B)^{-1} \tag{28}$$

The parallel plate interference formula expresses the addition of waves that pass through the interface directly, reflected twice inside the jet and transmitted after, reflected four times before transmission and so on. There is a time delay between the ray paths inside the jet and outside the jet which is given by Δt. The phase change $\omega\Delta t$ is

$$\phi_1=\omega\Delta t=4bk_B\left\{\frac{1}{\sin\delta_B}-\cot\delta_B\cos\delta_B\right\}=4bk_Cw \tag{29}$$

The addition of amplitudes T, $T\mathfrak{R}^2e^{i\phi_1}$, $T\mathfrak{R}^4e^{2i\phi_1}$, leads to the transmitted amplitude $T/(1-\mathfrak{R}^2e^{i\phi_1})$.

Because only the root mean square pressure is measured in the far field, the transmission factor is the modulus of the preceding expression. Therefore,

$$I=[T^2/(1+\mathfrak{R}^4-2\mathfrak{R}^2\cos\phi_1)]^{1/2} \tag{30}$$

In this expression, δ_B and δ_C are to be taken at the stationary values corresponding to w_s in Eq. (24). A modification of Eq. (30) may be more realistic if the turbulent boundaries of a real jet flow produce enough random fluctuations of $\cos\phi_1$ to eliminate the $\cos\phi_1$ factor. This effect may be expected to occur at very high frequencies when the wavelength of sound is of the same order as the random displacements of the interface. Therefore, at extremely high values of k_Cb,

$$I=[T^2/(1+\mathfrak{R}^4)]^{1/2} \tag{31}$$

Equation (31) also applies for extremely shallow angles near grazing incidence even at moderate values of k_Cb, because in this case small changes of jet width can produce large changes of path length.

Equations (30) and (31) that describe the parallel beam interference phenomenon are applicable for any angle of incidence δ_B, for a nonspreading jet. A simple modification of the preceding equations that is physically more realistic for a spreading jet is to restrict the zone of applicability of these equations to $0\le\delta_C\le\pi/2$ and set $I(\delta_C)=I(\pi/2)$ for $\delta_C\ge\pi/2$. The reason for this modification is simply that for waves traveling downstream from the nozzle exit, the parallel jet approximation is good. However, for waves traveling upstream, from downstream infinity, there is no amplitude addition because the jet is no longer of constant diameter far downstream. Equation (30) will be used with this modification. It is interesting to note that if δ_C is not restricted to values less than $\pi/2$, the angular directivity exhibits a cusp at the angle given by

$$\cos^2\theta=(1-M_B^2)/[(M_B^2+M_B-1)^{-2}-M_B^2] \tag{32}$$

The small local maximum at the cusp is not visible at low Mach numbers because it occurs too close to 90 deg where the levels rapidly approach zero.

Reflected Waves

The reflected waves are produced by the near-field pressure which is the contribution to the integral for p_B in Eq. (12) from values of $w>w_{\max}$. It is seen from Eq. (17) that $k_r=k_B\sin\delta_B=k_Cw$ which varies from $k_C/\sqrt{1-M_B^2}$ to ∞. Therefore, the near-field pressure at the nozzle exit plane, at $z=0$ indicated by a caret takes the form

$$\hat{p}_B(r)=\int_{k_C/\sqrt{1-M_B^2}}^{\infty} i^{-m}\chi(k_r)J_m(k_rr)k_r\,dk_r \tag{33}$$

This near-field pressure exists for both $r\le b$ and $r>b$. The part where $r\le b$ generates reflected waves that propagate inside the pipe. However, outside the pipe, the near-field decays and no radiation to infinity occurs. The radiated field generated from the near-field is symmetric upstream and downstream. Also, there is no radiation in the forward hemisphere. From this it is inferred that there is no backward reflected radiation outside the pipe. It can be shown[10] that the reflected wave motion in the pipe is given by

$$p_{\text{ref}}=\sum_{t=0}^{n_c}\frac{2J_m(\alpha_{mt}r/b)\alpha_{mt}^2}{b^2J_m^2(\alpha_{mt})(\alpha_{mt}^2-m^2)}$$
$$\times\int_0^b\hat{p}_B(r)J_m\left(\frac{\alpha_{mt}r}{b}\right)r\,dr\exp i(k_{mt}z+m\phi-\omega t) \tag{34}$$

Here k_{mt} is given by Eq. (4) with the negative square root. The number n_c is the last propagating mode before cutoff.

The reflected waves and the reflection amplitudes are dependent on M_A for two reasons. The first is that as M_B increases, the contribution of $\hat{p}_B(r)$ in Eq. (33) decreases. As $M_B\to 1$, the near-field vanishes and all the incident sound is radiated without reflection. The second reason that the reflection depends on M_B is because as the flow increases, more modes cut on and propagate. The total reflected power exhibits jumps as more modes cut on. In the case with no flow, Cho[4] has calculated reflections that exhibit such jumps as the frequency is varied and these curves agree well with those calculated by the Wiener-Hopf technique.[5]

Comparison with Other Theories and with Annular Flow Experiments

The angular directivity predicted by Eq. (26) for plane waves is compared in Fig. 2 with the theoretical results of Savkar[2] and the experimental data of Plumblee and Dean,[11] both of which are taken from Fig. 6 of Savkar's paper. Unfortunately, this comparison is not the best possible because the experimental data do not correspond to the case of a simple round jet but of sound propagating in an annulus of radius ratio of 0.566 ending abruptly at the exit. Since there was no sound in the central zone at the exit plane, it would be expected that calculations based on the present theory would indicate a radiation pattern shifted to higher angles from the jet axis in a manner similar to that exhibited by the higher modes in a circular pipe.

Savkar expected that the turbulent scattering that is not modeled in his theory would smooth the cusped lobe of his theoretical directivity in such a manner as to produce the smooth lobe shown by the experiment. However, it is noted that the present theory, which is based simply on plane wave refraction, produces better agreement with the experimental data without any recourse to turbulent scattering. The predictions based on both theories as well as Cho's formulation (in which the intuitive phonon concept is used) agree when there is no flow. However the agreement is not good with Cho's theory at 90 deg. In Fig. 1, within the refraction zone near the jet axis, multiple beam interference lobes may

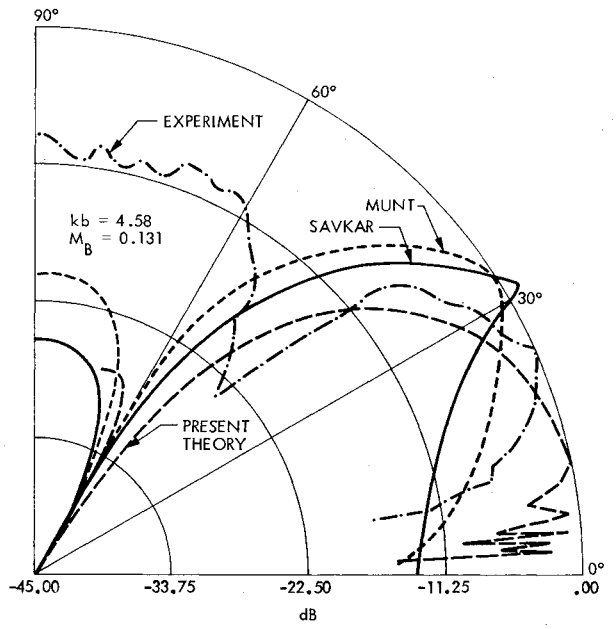

Fig. 2 Comparison of various theories with the experimental directivity obtained by Plumblee and Dean for plane waves transmitted through an annular jet of Mach number equal to 0.131; the frequency parameter $kb = 4.58$.

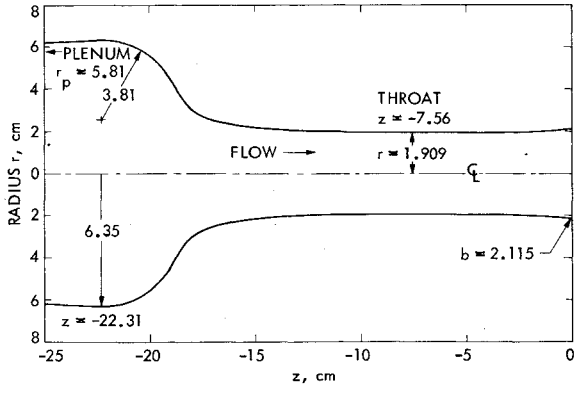

Fig. 3 Shape of the nozzle used in the present experiments.

be observed in the results of the present theory. These lobes can be smoothed out in reality by fluctuating flows associated with turbulence. Near 90 deg, results of the present theory show sound levels considerably below the experimental values, as do the calculations using Savkar's theory. The minimum predicted value of the sound occurs at about 60 deg; whereas, the experimental minimum is at about 45 deg. The minimum based on Savkar's theory is at about 60 deg. Munt's result is also shown in Fig. 2 and this agrees better with the experimental data in the refraction zone than Savkar's result.

Comparisons with Present Circular Flow Experiments

The experiments were conducted using nitrogen gas at room temperature. The flow, from a high-pressure supply, passed through electropneumatic transducers and into a plenum before discharging through a nozzle into an anechoic chamber. The length of this plenum was 1 m and the diameter was 11.6 cm. A convergent-divergent nozzle, which had a contour designed for a constant pressure gradient flow, was used at stagnation pressures that provided subsonic velocities at the nozzle exit. The throat diameter of the nozzle was 3.81 cm and the exit diameter was 4.23 cm. The shape of the nozzle that was used is shown in Fig. 3. The section downstream of the throat does not differ appreciably from a straight pipe. Pure tones were generated by the electropneumatic transducers that produced sound waves in the plenum. The

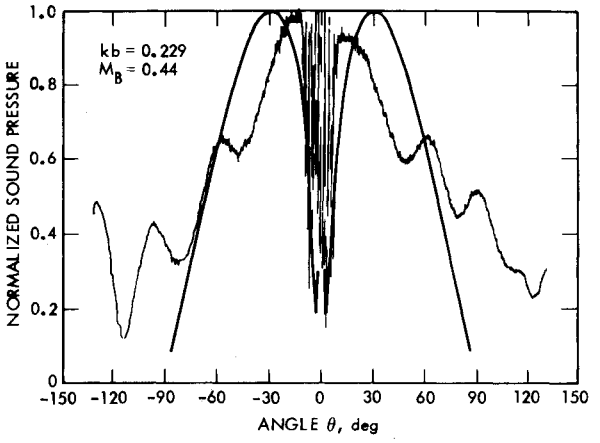

Fig. 4 Comparison of theoretical far-field angular distribution of sound with experimental data for a sound jet; $kb = 0.229$, $M_B = 0.44$.

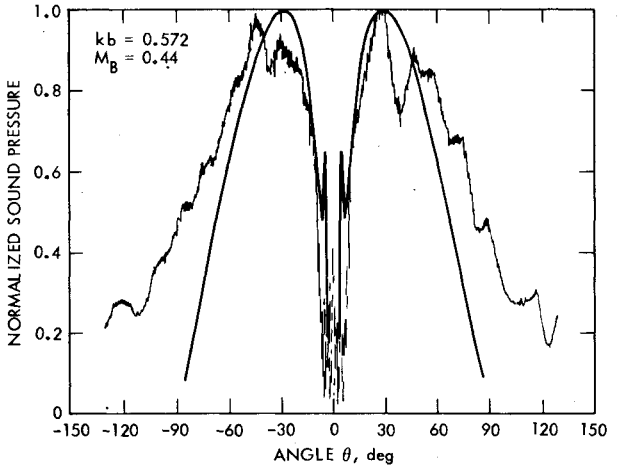

Fig. 5 Comparison of theoretical far-field angular distribution of sound with experimental data; $kb = 0.572$, $M_B = 0.44$.

radiated sound field was measured by a traversing microphone located 124 cm from the nozzle exit. The apparatus is described in greater detail in Ref. 12.

The apparatus was designed to study the transmission of low-frequency sound waves through the jet flow. However data were acquired over a wide range of frequencies, from 200 to 4000 Hz, which correspond to values of kb from 0.075 to 1.51. Since the theory is asymptotic, it is not clear how large kb should be for the theory to apply. Therefore, the data at all available frequencies have been used for comparison.

In the plenum, the first higher (1,0) mode can propagate when kb_p exceeds 1.84 (Morse and Ingard[9]). The quantity b_p, the radius of the plenum, is equal to 5.8 cm. Therefore, when kb exceeds $1.84\, b/b_p = 0.67$, higher modes can occur. Because the modal distributions in the duct and nozzle exit were not measured directly, data for kb larger than 0.67 are not reliable even though it is expected that with smooth duct transitions and with sources of sound located far upstream, the contamination from higher modes is small. It is worth noting that if higher modes were present, the effect would be to add to the radiation away from the jet axis and as a consequence widen the range of refraction. The best tests for the theory are those comparisons with the present data for which kb was less than 0.67.

The comparisons are shown in Figs. 4-6; many more are shown in Ref. 10. The ordinates in all these figures are normalized so that the maximum value is unity because in this case only the shapes of the directivity curves are being compared. The scales are linear. The experimental curves are obtained by traversing a single microphone on a boom that scanned the sound field slowly at a fixed radial distance equal

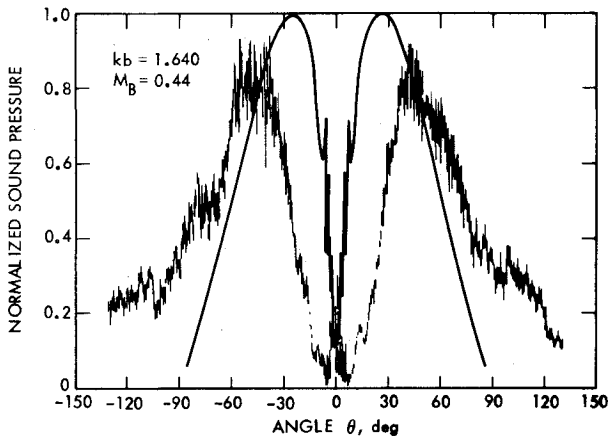

Fig. 6 Comparison of theoretical far-field angular distribution of sound with experimental data; $kb = 1.640, M_B = 0.44$.

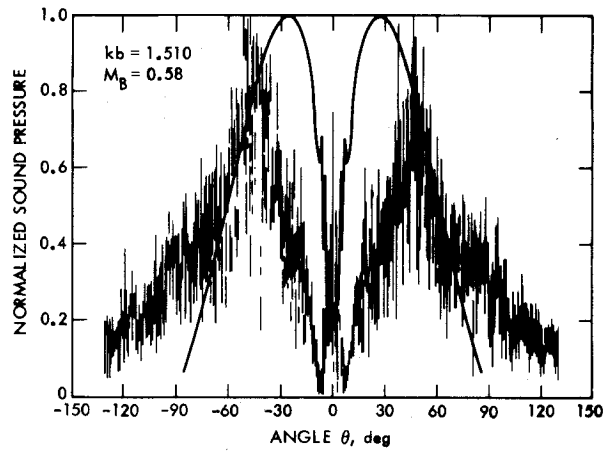

Fig. 7 Comparison of theoretical far-field angular distribution of sound with experimental data; $kb = 1.510, M_B = 0.58$.

to 124 cm. These curves also exhibit spatial waves associated with small reflections that exist even in an anechoic chamber. When the microphone crosses the jet flow, it is subject to wind noise which produces a large fluctuating signal that can be seen in all the figures. The fit between theory and experiment is surprisingly good in the refraction zone in Figs. 4 and 5 in which values of kb were less than 0.67. In all instances in these figures the jet exhaust Mach number was equal to 0.44. Near 90 deg, the predicted values are smaller than the experimental values. In Fig. 6 which is for kb larger than 0.67, the widths of the refraction zones are predicted to be too narrow.

The effect of changing flows at a fixed frequency were seen to be rather small for the three Mach numbers 0.21, 0.38, and 0.58. In Fig. 7 the experimental plots are very noisy because at this high frequency (4 kHz), the electropneumatic transducers are inefficient generators of sound and in addition the jet noise is large. Data which is not shown here, obtained at $M_B = 0.65$ show similar trends but are noisier.

In the theory the high-frequency formulas were used to describe refraction and therefore the changes in the valley of refraction are rather small. The only reason that there are changes in this zone at all is because the interference factor I, in Eq. (30), depends on the phase ϕ_1, which in turn depends on the frequency.

Comparison with the Experimental Results of Pinker and Bryce

Experimental results of Pinker and Bryce[13] on the far-field directivity of plane sound waves transmitted through a cold jet flow exhausting from a nozzle are compared with the present theory in Figs. 8 and 9. The presence of the nozzle has only a secondary influence of the radiated field as implied by

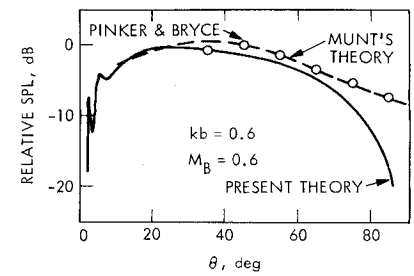

Fig. 8 Comparison of present theoretical directivity with the experimental data of Pinker and Bryce, and with theoretical results of Munt; $kb = 0.6, M_B = 0.6$.

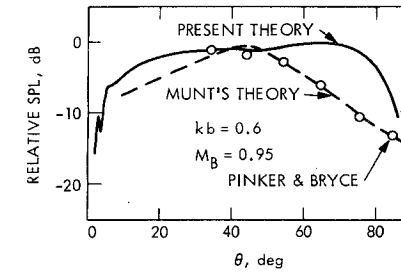

Fig. 9 Comparison of present theoretical directivity with the experimental data of Pinker and Bryce, and with theoretical results of Munt; $kb = 0.6, M_B = 0.95$.

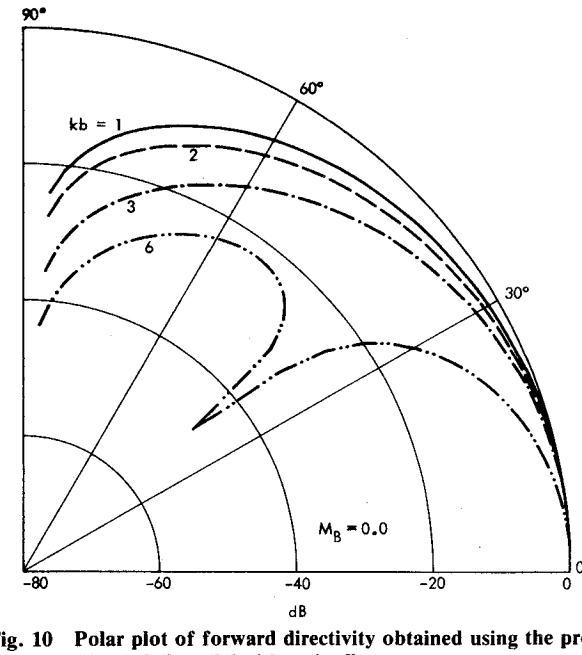

Fig. 10 Polar plot of forward directivity obtained using the present theory at $kb = 1, 2, 3$, and 6 with no jet flow.

the present analysis. The same data shows good agreement with Munt's[1] theoretical results over practically the whole range of angles greater than 30 deg. Unfortunately, there are no experimental data for angles less than 30 deg where the deep refraction dip occurs. This is the zone where theories and experiment tend to disagree most.

The experimental results exhibit an increase in radiation at low angles with increasing M_B. Ffowcs Williams et al.[14] predicted that low-frequency sound from a nozzle has a directivity proportional to $(1 + 2M_B\cos\theta)$. Experimental data obtained in the present experiments (some of which are not shown here) indicates that the far-field sound pressure is proportional to $(1 + 2M_B\cos\theta)/(1 - M_B\cos\theta)^{\alpha}$ with $\alpha = 2\exp - 4k_C b$. It was observed that $(1 - M_B\cos\theta)^{-\alpha}$ was also a good fit to the experimental data over the range of M_B

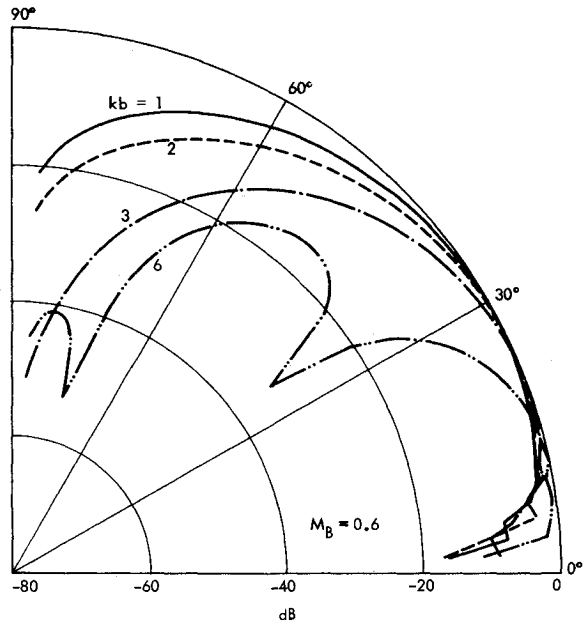

Fig. 11 Polar plot of forward directivity predicted by use of the present theory at $kb = 1, 2, 3$, and 6 at a jet Mach number $M_B = 0.6$.

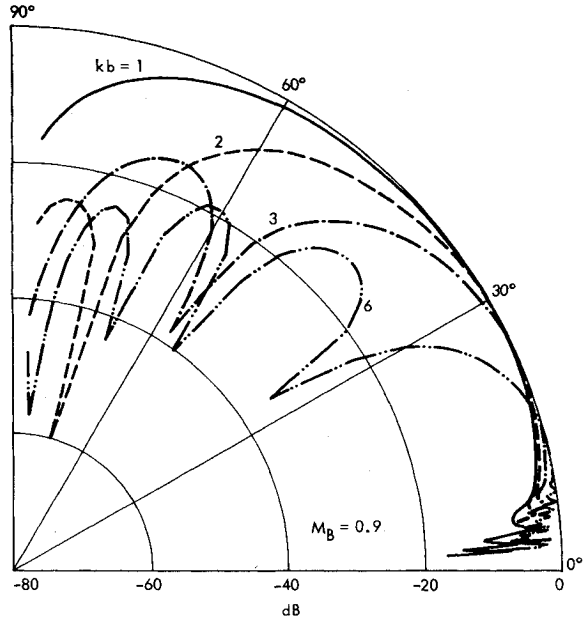

Fig. 12 Polar plot of forward directivity obtained using the present theory at $kb = 1, 2, 3$, and 6 at a jet Mach number $M_B = 0.9$.

investigated. The low-frequency convection amplification factor $(1 - M_B\cos\theta)^{-2}$ disappears at high values of $k_C b$ in contrast to the theoretical prediction of Mani[3] which contains a frequency independent factor. This empirical factor seems to be consistent with the experimental data in Figs. 8 and 9. The present theory does not contain this factor and, as a consequence, a low-frequency directivity that tends to be almost omnidirectional at high Mach numbers is obtained. It is not clear whether the factor $(1 + 2M_B\cos\theta)$ would be present at still higher frequencies than those used in the empirical correlation (i.e., $k_C b = 0.572$). In any case, it is clear from the figures that the present theory does not apply at low frequencies because the low-frequency directivity factor is left unaccounted for by this geometrical acoustics theory. At low Mach numbers, however, where the preceding factor is small, the forward directivity is predicted satisfactorily. In all cases, the sound pressure in the refraction zone is predicted realistically.

Additional Theoretical Results

The theoretical directivity given in Eq. (26) is plotted in Figs. 10-12 for the Mach numbers 0 and 0.9 at four values of kb equal to 1, 2, 3, and 6 to exhibit the changes caused by flow. At $M_B = 0$, there is a reduction in radiation at higher angles as kb increases. At high values of kb, additional lobes occur. In Figs. 11 and 12 the refraction zone near the jet axis can be seen. Radiation at large angles is reduced by the flow. The distribution outside the refraction zone becomes steeper in the forward direction. At a Mach number equal to 0.9, many more lobes are evident as shown in Fig. 12 because of the large variations in the factor $(1 - M_B^2\sin^2\theta)^{-1/2}$ in the argument of the Bessel function in Eq. (26).

The results of the present theory disagree substantially with the trends indicated by Mani's[3] theory for the two-dimensional case, at high Mach numbers. At a Mach number equal to 0.9, Mani's[3] theory exhibits an extremely steep maximum on the jet axis with the sound levels falling by 20 dB at about 30 deg at kb values equal to 1.25, 3.75, and 6.25. In all cases, there are no refraction valleys at the jet axis. At $kb = 3.75$ there are two frontal lobes as in Fig. 11; but at $kb = 6.25$, Mani's result shows only one lobe, whereas the present theory exhibits four lobes. The convective amplification that is present in Mani's theory and that accounts for such a strong forward radiation does not appear in the present theory. In addition the diffraction argument $k_C b\sin\theta(1 - M_B^2\sin^2\theta)^{-1/2}$ of the present theory is accounted for by different factors in Mani's theory that exhibits different lobe structures particularly as M_B tends to unity. In Ref. 10, directivities at $M_B = 0.3$ and 0.6 are also shown.

Summary and Conclusions

The general expressions for the transmission and reflection of a spinning sound wave moving through a jet flow were derived by a theory in which the high-frequency laws were used to describe refraction and reflection at the boundary between the slug flow jet and the ambient atmosphere. The results of this theory for the plane wave case were compared with other theories and with experiments over a range of flow Mach numbers up to 0.65. The frequency parameter was varied from 0 to 1.64. The agreement with experiment was better than that shown by Savkar's[2] theory. The present theory agrees with other theories at zero Mach number. As the pipe exit Mach number increases toward unity, the results of the present theory disagree increasingly from Mani's theory. In particular, the strong convective amplification associated with moving sources that eliminates the shallow refraction dip near the jet axis at high Mach numbers in Mani's theory is completely absent. Available experimental data up to a Mach number equal to 0.65 show that the deep refraction dip near the jet axis exists at all frequencies and does not show large changes with variations in jet velocity. The present high-frequency theory does not contain the low-frequency factor $(1 + 2M_B\cos\theta)$ of the Ffowcs Williams[14] theory, which is exhibited by the experimental data of Pinker and Bryce.[13] Experiments indicate that the convection amplification factor is frequency dependent and is $(1 - M_B\cos\theta)^{-\alpha}$ where $\alpha = 2\exp - 4k_C b$. Therefore, the results of the present theory disagree with the Pinker and Bryce data, at Mach numbers near unity. It is concluded that even though the present theory is much more simplified than the more complex theories that make use of the Wiener-Hopf technique, the results of comparison with experiment are satisfactory at Mach numbers up to 0.65, even at low frequencies.

Appendix: Correction to the Radiated Field at Low Frequencies

A significant improvement in the theory can be achieved by including the contribution to the forward radiation from the large near-field pressure that occurs at low frequencies. Equation (33) expresses the near-field pressure $\hat{p}_B$, at the pipe

exit. A portion of this field, which corresponds to the plane wave mode of magnitude $\langle \hat{p}_B \rangle$, is propagated into the pipe as a reflected wave. The angular bracket denotes the average value over the pipe cross section. Thus,

$$\langle \hat{p}_B \rangle = \int_0^b \hat{p}_B(r) r dr \Big/ \int_0^b r dr \tag{A1}$$

The remaining field $\{p_B - \langle \hat{p}_B \rangle\}$ is radiated. The Hankel transform of the corrected pressure field is, therefore, given by

$$\chi(k_r) + \chi_1(k_r) = \int_0^b \{p_B(r) + \hat{p}_B(r) - \langle \hat{p}_B(r) \rangle\} J_m(rk_r) r dr \tag{A2}$$

On replacing $\chi(k_r)$ in Eq. (20) by the corrected quantity $\chi(k_r) + \chi_1(k_r)$, the new pressure-field amplitude is determined by the equations

$$p = -f(w_s)[-2\pi/h''(w_s)R]^{1/2} \tag{A3}$$

where

$$f(w_s) = \{\chi(k_C w_s) + \chi_1(k_C w_s)\} I(w_s) k_C^2 w_s \times (2\pi w_s k_C R \sin\theta)^{1/2} \tag{A4}$$

In the preceding equation

$$h''(w_s) = -[k_C/(\cos^2\theta)](1 - M_B^2 \sin^2\theta)^{1/2} \tag{A5}$$

and w_s is given by Eq. (24).

Thus, Eqs. (A3-A5) replace Eq. (25), which is a high-frequency approximation. Even though results are not presented, it can be verified that the corrected results will exhibit convective amplification at low frequencies and, therefore, increase the radiation at low angles (θ) outside the refraction zone.

Acknowledgments

This paper represents one phase of research performed by the Jet Propulsion Laboratory, California Institute of Technology, sponsored by NASA Contract NAS7-100. The discussions held with P. Massier regarding this task are greatly appreciated.

References

[1] Munt, R. M., "The Interaction of Sound With a Subsonic Jet Issuing from a Semi-Infinite Cylindrical Pipe," *Journal of Fluid Mechanics*, Vol. 83, Pt. 4, 1977, pp. 609-640.

[2] Savkar, S. D., "Radiation of Cylindrical Duct Acoustic Modes with Flow Mismatch," *Journal of Sound and Vibration*, Vol. 42, No. 3, 1975, p. 363.

[3] Mani, R., "Refraction of Acoustic Duct Waveguide Modes by Exhaust Jets," *Quarterly of Applied Mathematics*, Vol. 30, Jan. 1973, pp. 501-520.

[4] Cho, Y. C., "A Statistical Theory for Sound Radiation and Reflection from a Duct," *Journal of the Acoustical Society of America*, Vol. 65, June 1979, pp. 1373-1379.

[5] Levine, H. and Schwinger, J., "On the Radiation of Sound from an Unflanged Circular Pipe," *Physical Review*, Vol. 73, No. 4, 1948, p. 383.

[6] Brekhovskikh, L. M., *Waves in Layered Media*, Academic Press, New York, 1960, Chap. I.

[7] Lighthill, J., *Waves in Fluids*, Cambridge University Press, Cambridge, 1978, Sec. 1.12.

[8] Stratton, J. A., *Electromagnetic Theory*, McGraw Hill Book Co., New York, 1941, pp. 370-371.

[9] Morse, P. M. and Ingard, K. U., *Theoretical Acoustics*, McGraw Hill Book Co., New York, 1968, p. 511.

[10] Parthasarathy, S. P. and Vijayaraghavan, A., "Transmission of High Frequency Sound Waves Through a Slug Flow Jet," AIAA Paper 80-0969, presented at the AIAA 6th Aeroacoustics Conference, Hartford, Conn., June 1980.

[11] Plumblee, H. E. and Dean, P. D., "Sound Measurements within and in the Radiated Field of an Annual Duct with Flow," *Journal of Sound and Vibration*, Vol. 28, Pt. 4, 1973, pp. 715-735.

[12] Parthasarathy, S. P., Cuffel, R. and Massier, P. F., "Influence of Internally Generated Pure Tones on the Broadband Noise Radiated from a Jet," *AIAA Journal*, Vol. 16, May 1978, pp. 538-540.

[13] Pinker, R. A. and Bryce, W. D., "The Radiation of Plane Wave Duct Noise from a Jet Exhaust, Statically and in Flight," AIAA Paper 76-581, presented at the 3rd Aeroacoustics Conference, Palo Alto, Calif., July 1976.

[14] Ffowcs Williams, J. E., Leppington, F. G., Crighton, D. G., and Levine, H., "Papers on Novel Aerodynamic Noise Source Mechanisms at Low Jet Speeds," Aeronautical Research Council, Current Paper 1195, 1972, Chap. 2.